Editors' Suggestion

Mass Changes the Diffusion Coefficient of Particles with Ligand-Receptor Contacts in the Overdamped Limit

Sophie Marbach[1,2,*] and Miranda Holmes-Cerfon[1,†]
[1]Courant Institute of Mathematical Sciences, New York University, New York 10012, USA
[2]CNRS, Sorbonne Université, Physicochimie des Electrolytes et Nanosystèmes Interfaciaux, F-75005 Paris, France

(Received 9 December 2021; revised 29 March 2022; accepted 22 June 2022; published 21 July 2022)

Inertia does not generally affect the long-time diffusion of passive overdamped particles in fluids. Yet a model starting from the Langevin equation predicts a surprising property of particles coated with ligands that bind reversibly to surface receptors: heavy particles diffuse more slowly than light ones of the same size. We show this by simulation and by deriving an analytic formula for the mass-dependent diffusion coefficient in the overdamped limit. We estimate the magnitude of this effect for a range of biophysical ligand-receptor systems, and find it is potentially observable for tailored micronscale DNA-coated colloids.

DOI: 10.1103/PhysRevLett.129.048003

It is well known that inertia does not affect either the equilibrium probabilities or dynamics in overdamped systems [1], and especially that it does not affect the long-time single-particle diffusion coefficient of micronscale particles in liquids at equilibrium [2]. Momentum relaxation for micronscale particles occurs over a timescale $\tau_m \simeq 1\ \mu$s (see Supplemental Material [3], Sec. 3.1), while particles are generally observed on much longer timescales, where the equilibrium motion is diffusive with diffusion coefficient independent of mass for large enough particles [4,5]. Inertia can only affect the short-time mobility of a particle [2,5], and it can play a role for active particles where τ_m is comparable to the diffusive rotational timescale, which is experimentally accessible only in air [6]. To our knowledge, there is currently no proposed physical system where inertia could affect the long-time single-particle diffusion of micronscale particles in liquids at equilibrium.

Yet, the overdamped dynamics of particles with ligand-receptor contacts, such as colloids functionalized with DNA [7–9], viruses [10–13], or white blood cells [14–16] are not fully understood. Such particles are coated with sticky ligands that bind and unbind to receptors on an opposing surface, changing the particle's mobility [8,10,17,18]. The ligand binding and unbinding rates can be fast, in some cases comparable to $1/\tau_m$ [19,20]. One might speculate that when binding occurs on the same timescale as the relaxation of the ambient fluid's momentum, the coupling between binding dynamics and momentum relaxation could lead to inertial effects at longer timescales [2,4–6,21–27]. For example, bimolecular reactants with inertia can show different survival probability decay functions depending on their mass [28,29]. Furthermore, we have recently pointed out that models of DNA-coated colloids find different long-time diffusion coefficients when they start with the underdamped Langevin equation for particle motion [30] (Fig. 1, dotted line) or from the overdamped equation [20] (Fig. 1, dashed line). We therefore ask: could inertia affect the long-time diffusion of particles with ligand-receptor contacts?

Here, we shift the common perspective on overdamped systems by showing that the long-time diffusion coefficient of particles with ligand-receptor contacts depends on mass. We investigate a minimal model for such particles that includes the essential ingredients of (i) inertial relaxation and (ii) stochastic dynamics of binding and unbinding. We consider an N-legged particle of mass m, with springlike "legs" representing the ligands [31–33], and a "sticker" at the tip of each leg that may transiently attach to a uniformly

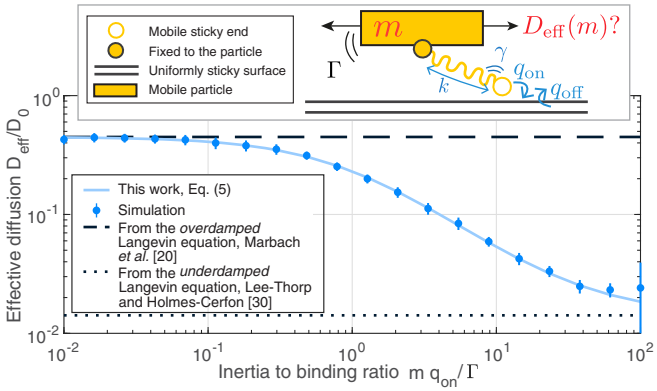

FIG. 1. Mass changes the diffusion coefficient of a particle with 1 ligand. Top: Sketch of a particle of mass m with a single ligand (leg); other parameters described in text. Bottom: Long-time diffusion coefficient $D_{\rm eff}$ of the particle as a function of inertia to binding timescale ratio $mq_{\rm on}/\Gamma$, obtained from stochastic simulations of Eqs. (1)–(3) and compared with analytic results, as described in legend. Error bars are one standard deviation for 20 independent simulations, with $q_{\rm on} = 0.01\ k/\Gamma$, $q_{\rm off} = 0.008\ k/\Gamma$, $\gamma = \Gamma$.

sticky surface (Fig. 1, inset). Using standard coarse-graining techniques [20,34,35], we derive an analytic expression, verified by simulations, that shows the long-time diffusion coefficient $D_{\mathrm{eff}}(m)$ decreases with mass (Fig. 1, blue line). This inertial slowdown occurs when the binding timescale is comparable to the inertial timescale, with a magnitude increasing with leg stiffness and decreasing with N, and we show it could potentially be measured in DNA-coated colloids with targeted experiments.

Our model starts with the approach we introduced for overdamped dynamics in Ref. [20], that, as we have shown, reproduces the experimentally observed diffusion of certain DNA-coated colloids. We modify the model to include a dependence on mass. The particle's motion is investigated in 1D on the lateral dimension parallel to the surface. Legs attach and detach independently to the surface with constant rates q_{on}, q_{off}. When unbound, the leg lengths l_j evolve according to

$$\frac{dl_j}{dt} = -\frac{k}{\gamma}(l_j - l_0) + \sqrt{\frac{2k_BT}{\gamma}}\eta_j, \tag{1}$$

where k is a spring constant [31–33], l_0 is a rest length, and γ is the friction coefficient of each leg. The η_j are uncorrelated white Gaussian noises, such that $\langle \eta_j(t)\eta_k(t)\rangle = \delta_{kj}\delta(t-t')$ and $\langle \eta_j(t)\rangle = 0$, where $\langle\cdot\rangle$ is an average over realizations of the noise. Inertia of the legs may be neglected as, in general, legs are much lighter than the particle (see Supplemental Material [3], Sec. 2.4). When bound, the legs are constrained to move at the same speed as the particle, $v = dx/dt$, where x is the particle position

$$\frac{dx}{dt} = \frac{dl_i}{dt} = v. \tag{2}$$

Finally, the particle's velocity is governed by Newton's law, including friction Γ and stochastic forces $\sqrt{2k_BT\Gamma}\eta_x$ induced by the ambient fluid, as well as friction, recoil, and stochastic forces originating from the bound legs:

$$m\frac{dv}{dt} = -\Gamma v + \sqrt{2k_BT\Gamma}\eta_x + \sum_{i\in\mathrm{bound}}(-\gamma v - k(l_i - l_0) + \sqrt{2k_BT\gamma}\eta_i). \tag{3}$$

In the absence of legs, the particle diffuses with a bare diffusion coefficient $D_0 = k_BT/\Gamma$. The hydrodynamic friction coefficient Γ depends on the distance to the wall and may be obtained from lubrication theory [36,37] or from measurements [38]. Here, the η_i and η_x are further uncorrelated white Gaussian noises and i is a running index over currently bound legs. For a particle in a fluid the relevant mass scale in Eq. (3) is $m \to m + m_f/2$, where m_f is the mass of the displaced volume of fluid [2,39]. We remark that in contrast to previous models [20,40], here it is not necessary to project the unbound stochastic dynamics to obtain the bound dynamics; Newton's law is sufficient. All parameters of the model, including the binding rates, may depend on temperature T, which we assume to be constant.

The Langevin dynamics in Eq. (3) are a common starting point to investigate the effect of inertia [25,41]. Although these equations imply an exponential decay of momentum, which is faster than the algebraic decay that occurs in fluids of similar density as the particle, as envisioned here [2], we expect our model will give a lower bound on the effect of inertia and is therefore suited to explore the onset of inertial effects.

Stochastic simulations of our model show that the long-time diffusion coefficient D_{eff} of the particle depends on the particle's mass (see simulation details in Supplemental Material, Sec. 1, building on Ref. [42]). For example, Fig. 1 shows that D_{eff} for a 1-legged particle continuously decreases with mass, by more than an order of magnitude, from the overdamped [20] to the underdamped [30] regimes.

To further understand how this decrease depends on model parameters $(m, N, k, q_{\mathrm{on}}, q_{\mathrm{off}}, \gamma, \Gamma)$, we derive an analytic expression for D_{eff} by considering the overdamped limit of the combined particle and leg dynamics. We introduce the five nondimensional scales:

$$x \to L_x\tilde{x}, \quad l_i - l_0 \to L\tilde{l}_i, \quad t \to \tau\tilde{t}, \quad v \to V\tilde{v}, \quad m \to M\tilde{m}.$$

Here, $L = \sqrt{k_BT/k}$ is the characteristic length of leg fluctuations, while L_x and τ are respectively the length scale and timescale for the long-time motion of x. The latter two scales are not determined *a priori* by intrinsic scales [35,43], but rather are chosen large enough that coarse graining will lead to diffusive dynamics [20]. Hence, $L_x = L/\epsilon$, where $\epsilon \ll 1$ is a small nondimensional number, and $\tau = L_x^2/D_0$, which corresponds to $\tau = \Gamma/k\epsilon^2$. Velocity fluctuations are fast compared to diffusive motion such that $V = L_x/\tau\epsilon$. Importantly, we specify the scale of mass by considering that the velocity autocorrelation time in the absence of recoil forces, $\tau_v = \tau_m = M/\Gamma$, is small compared to the observation time, $\tau_v = \tau_m = \epsilon^2\tau$. This is the usual scaling to obtain *overdamped*, or more generally long-time diffusive, dynamics [34]. Finally, we observe the system at sufficiently long times that the remaining timescales are much shorter: $\gamma/k \sim \Gamma/k \sim q_{\mathrm{on}}^{-1} \sim q_{\mathrm{off}}^{-1}$, so that $q_{\mathrm{on}} \to (\tau/\epsilon^2)\tilde{q}_{\mathrm{on}}$ and similarly for q_{off}.

We use these scalings to coarse-grain Eqs. (1)–(3). Standard coarse-graining techniques [20,30,34,35,44] (see Supplemental Material, Sec. 2) show that the particle diffuses at long times with diffusion coefficient

$$D_{\mathrm{eff}}(m) = \frac{k_B T}{\Gamma_{\mathrm{eff}}(m)} = \sum_{n=0}^{N} p_n \frac{k_B T}{\Gamma_n(m)}, \tag{4}$$

where $p_n = \binom{N}{n}\{q_{\mathrm{on}}^n q_{\mathrm{off}}^{N-n}/[(q_{\mathrm{on}} + q_{\mathrm{off}})^N]\}$ is the probability to have n bonds and $\Gamma_n(m)$ are the effective friction coefficients for a state with n bonds. The $\{\Gamma_n\}$ satisfy a linear system of equations that is reported in Eq. (S2.23) in the Supplemental Material [3] and that depends on parameters $(m, N, k, q_{\mathrm{on}}, q_{\mathrm{off}}, \gamma, \Gamma)$. Importantly, Eq. (4) predicts up to order of magnitude changes on the effective diffusion D_{eff} depending on the specific microscopic parameter values.

Let us analyze in detail a $N = 1$-legged particle. The friction coefficients can be obtained analytically as

$$\begin{aligned} \frac{\Gamma_0(m)}{\Gamma} &= 1 + \frac{m q_{\mathrm{on}}}{\Gamma} \frac{\gamma_{\mathrm{eff}}}{\gamma_{\mathrm{eff}} + \Gamma + m(q_{\mathrm{on}} + q_{\mathrm{off}})}, \\ \frac{\Gamma_1(m)}{\Gamma} &= 1 + \frac{\gamma_{\mathrm{eff}}}{\Gamma} \frac{\Gamma + m q_{\mathrm{on}}}{\Gamma + m(q_{\mathrm{on}} + q_{\mathrm{off}})}. \end{aligned} \tag{5}$$

Here, $\gamma_{\mathrm{eff}} = \gamma + k[(1/q_{\mathrm{off}}) + (\gamma/k)(q_{\mathrm{on}}/q_{\mathrm{off}})]$ is the effective friction from the leg, including the leg's bare friction γ and recoil forces from the tethered spring. The coefficients satisfy $\Gamma_0 \leq \Gamma_1$ as, when it is bound, the leg exerts additional recoil forces on the particle, as was observed in a variety of systems, from rubber [45] to muscle friction [46] to virus motion on mucus [12]. We compare our analytic result for D_{eff} with direct stochastic simulations over a wide range of parameters and find excellent agreement (Fig. 1 and Fig. S1 in the Supplemental Material [3]). Overall, the effective friction Γ_{eff} increases with mass, and therefore the particle's diffusion slows down with increased mass.

Equation (5) gives insight into what controls both the onset of the diffusion slowdown and the magnitude of the effect. Diffusion begins to decrease when the binding and unbinding times $\tau_{\mathrm{on}} = q_{\mathrm{on}}^{-1}$, $\tau_{\mathrm{off}} = q_{\mathrm{off}}^{-1}$ become comparable with the relaxation time of inertia, $\tau_m = m/\Gamma$. This is apparent in Fig. 1, where the transition between limit regimes occurs for $m q_{\mathrm{on}}/\Gamma \sim 1$. For shorter binding times, $\tau_{\mathrm{on}} \sim \tau_{\mathrm{off}} \ll \tau_m$, inertial effects matter, and the friction coefficients for $m \gg \Gamma/q_{\mathrm{on}}, \Gamma/q_{\mathrm{off}}$ converge to

$$\frac{\Gamma_0^{m=\infty}}{\Gamma} = \frac{\Gamma_1^{m=\infty}}{\Gamma} = 1 + p_1 \frac{\gamma_{\mathrm{eff}}}{\Gamma}. \tag{6}$$

The friction coefficients are the same, regardless of the state (bound or unbound) of the particle. This is coherent: since the particle has significant inertia, it does not have time to accelerate or decelerate to a different dynamical regime upon changing state. Binding and unbinding happen too rapidly for the particle to sense the difference. Equation (6) was also obtained in Ref. [30] starting from the underdamped equations.

Reciprocally, if binding timescales are long compared to inertial relaxation ($\tau_{\mathrm{on}} \sim \tau_{\mathrm{off}} \gg \tau_m$) we expect inertia to play a negligible role: the particle has time to accelerate and reach an overdamped limit motion before any further change of state occurs. In this case the friction coefficients are

$$\frac{\Gamma_0^{m=0}}{\Gamma} = 1, \qquad \frac{\Gamma_1^{m=0}}{\Gamma} = 1 + \frac{\gamma_{\mathrm{eff}}}{\Gamma}. \tag{7}$$

Equation (7) was also obtained in Ref. [20], starting with overdamped equations for the particle.

We therefore find that the onset of inertial effects is governed by the ratio of timescales, $\tau_{\mathrm{on}} \sim \tau_{\mathrm{off}}$ compared to τ_m. *A posteriori*, it is natural that this onset is controlled by timescales, yet it was not obvious *which* of the diversity of timescales would matter. For example, the timescale for relaxation of leg fluctuations k/γ does not control the occurrence of inertial slowdown.

However, k/γ does control the magnitude of the inertial slowdown, via γ_{eff}. The relative slowdown between the underdamped and the overdamped regime is

$$\frac{D_{\mathrm{eff}}^{m=\infty}}{D_{\mathrm{eff}}^{m=0}} = \frac{1 + \frac{\gamma_{\mathrm{eff}}}{\Gamma}}{1 + \frac{\gamma_{\mathrm{eff}}}{\Gamma} + p_0 p_1 \frac{\gamma_{\mathrm{eff}}^2}{\Gamma^2}}. \tag{8}$$

If the leg is very stiff ($k \gg \Gamma q_{\mathrm{off}}$, implying $\gamma_{\mathrm{eff}} \gg \Gamma$), then diffusion can be significantly slowed for massive particles, $D_{\mathrm{eff}}^{m=\infty} \ll D_{\mathrm{eff}}^{m=0}$. Indeed, stiff legs greatly reduce motion in the bound state, $\Gamma_1 \gg \Gamma$. Since a heavy particle does not have the time to accelerate while its leg is unbound, we also have increased friction in the unbound state $\Gamma_0^{m=\infty} \gg \Gamma$ and the particle's overall mobility is decreased, by up to orders of magnitude (as seen in Fig. 1). For an overdamped particle, on the contrary, even with a stiff leg, the particle can still move when it is unbound, as it has time to accelerate ($\Gamma_0^{m=0} = \Gamma$), and its diffusion coefficient remains finite.

Let us now consider a particle with many legs involved in the binding process, say, $N \approx 100$–1000, as in some DNA-coated colloids at low temperatures [47,48]. When the average number of bonds is large, $\bar{N} = [q_{\mathrm{on}}/(q_{\mathrm{on}} + q_{\mathrm{off}})]N \gg 1$, the $\{\Gamma_n\}$ can be approximated by the averaged value $\Gamma_{\bar{N}}$ (see Supplemental Material [3], Sec. 2.3.4), yielding

$$\Gamma_{\mathrm{eff}}(m) \underset{\bar{N} \gg 1}{\simeq} \Gamma + \bar{N} \gamma_{\mathrm{eff}}. \tag{9}$$

The diffusion coefficient no longer depends on the mass of the particle. Stochastic simulations, as well as numerical solutions of the linear system satisfied by the $\{\Gamma_n\}$, confirm this result: the diffusion coefficient when N is large converges to a value independent of mass (Fig. 2). Interestingly, the transition to the slowed-down diffusion regime occurs when $\tau_m/\tau_{\mathrm{on}} \propto N$ (see Supplemental Material [3], Sec. 2.3.3).

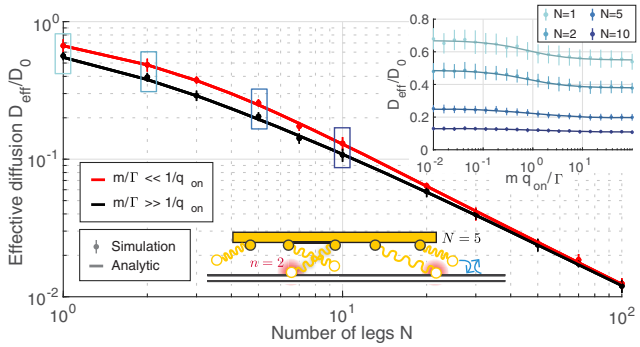

FIG. 2. Inertial slowdown vanishes with numerous legs. D_{eff} versus number of legs N, for large mass (black, $mq_{\mathrm{on}}/\Gamma = 100$) and small mass (red, $mq_{\mathrm{on}}/\Gamma = 0.01$), from stochastic simulations (markers) and from Eq. (4) (solid lines, solving numerically for $\{\Gamma_n\}$). Top inset: D_{eff} versus inertia to binding timescale ratio for various N. Bottom inset: Schematic of an N-legged particle including n surface-bound legs. Error bars are one standard deviation for 100 independent simulations, with $\gamma = 0.1\Gamma$, $q_{\mathrm{off}} = 0.8\ k/\Gamma$, and $q_{\mathrm{on}} = k/\Gamma$.

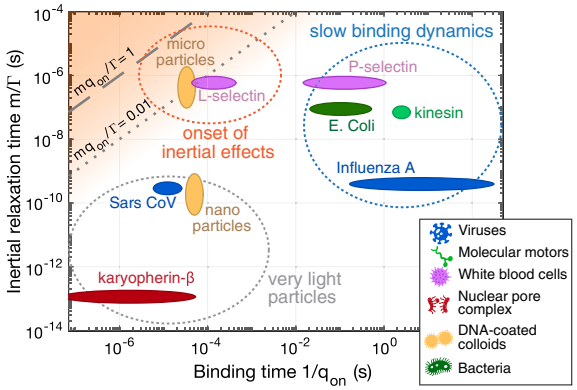

FIG. 3. Inertial effects in biophysical systems. Ashby chart comparing the inertia and binding timescales for various systems. The height and width of the filled ellipses represent the range of values found in the literature (see Supplemental Material [3], Sec. 3). All data is from measurements at room temperature, except for DNA-coated colloids whose parameters are taken at their respective melting temperatures [48]. Large dashed circles represent global categories of systems. The shaded orange area represents parameter values where inertial effects could be important.

Why do inertial effects vanish with a large number of legs? For a heavy particle, the friction coefficients for each bond state are equal [as in Eq. (6)]: $\Gamma_0^{m=\infty} = \Gamma_1^{m=\infty} = \ldots = \Gamma_N^{m=\infty} = \Gamma + \bar{N}\gamma_{\mathrm{eff}}$ (see Supplemental Material [3], Sec. 2.3.2), because the particle does not have time to accelerate between bond state changes, and hence is only sensitive to the average configuration. The difference is that now an average of $\bar{N}$ legs exerts extra recoil forces. For a very light particle, friction coefficients for each bond state are different, but their sum in Eq. (4) is dominated by the most likely state, which is $\bar{N}$ when this average is large, leading to $\Gamma_{\mathrm{eff}}^{m=0} \approx \Gamma_{\bar{N}}^{m=0} = \Gamma + \bar{N}\gamma_{\mathrm{eff}}$. Numerous legs can thus be thought of as self-averaging, and hence transitions between states do not matter as much as when there are a small number of bound legs.

We now explore the possible emergence of such inertial effects in biological or biomimetic systems where a small average number of bound legs $\bar{N} \simeq 1$ is inherent, or can be achieved, e.g., with temperature control [48]. To observe inertial effects, the binding times ($\tau_{\mathrm{on}} = q_{\mathrm{on}}^{-1}$, $\tau_{\mathrm{off}} = q_{\mathrm{off}}^{-1}$) have to be faster than the inertial relaxation time $\tau_m = m/\Gamma$. As typical adhesive systems have $q_{\mathrm{off}} \lesssim 10 q_{\mathrm{on}}$, we focus on q_{on}. We report in Fig. 3 the orders of magnitude for the momentum relaxation time $\tau_m = m/\Gamma$ and binding times $\tau_{\mathrm{on}} = q_{\mathrm{on}}^{-1}$ for a variety of particles with ligand-receptor contacts using data available in the literature [13,19,32,47–80] (recapitulated in Supplemental Material [3], Sec. 3.2).

Numerous ligand-receptor systems have binding kinetics that are too slow to observe inertial effects, with $q_{\mathrm{on}} \lesssim 100\ \mathrm{s}^{-1}$ (blue dashed circle in Fig. 3), e.g., spike proteins on the Influenza A virus [49,50], molecular motors transporting cargos [81], and pili adhesion of Escherischia Coli [65–67].

Other systems have fast binding kinetics ($q_{\mathrm{on}} \gtrsim 10^4\ \mathrm{s}^{-1}$), but not fast enough to incur inertial effects on the lighter systems they are connected to (gray dashed circle in Fig. 3). These often correspond to smaller particles, and since $m/\Gamma \propto R^2$, this decreases the maximum binding timescale required to observe inertial effects. Examples include Sars CoV 1 and 2 viruses [79,80], DNA-coated nanocolloids [53], and protein transporters in the nuclear pore complex [73].

Inertial effects may occur for two systems with a specific combination of large particles and fast binding kinetics (orange dashed circle in Fig. 3): (i) micron-sized DNA-coated colloids near their melting temperature and (ii) white blood cells with adhesion mediated by L-selectin. For both systems, typical existing experimental designs possess an inertia to binding timescale ratio $mq_{\mathrm{on}}/\Gamma \simeq 10^{-3} - 10^{-1}$, which is close to the range where we predict inertial slowdown.

DNA-coated colloids offer a promising route to probe such inertial slowdown, as they may be finely tuned by changing their size, coating density, ligand length, material composition, etc., and to observe diffusion over several degrees [20,51]. We speculate that inertial effects could be observed by solving the challenge of building such colloids with different cores [54,82] but keeping the surface DNA coatings the same: using a gold [47] or a polystyrene [48] core to make a heavy or a light particle, respectively.

To maximize inertial effects, one must increase both mq_{on}/Γ, to reach the transition between the noninertial and inertial regimes, and $\gamma_{\mathrm{eff}}/\Gamma$, to increase the magnitude of the slowdown; see Eq. (8). The latter ratio, in DNA-coated colloids, is typically dominated by the term $k/\Gamma q_{\mathrm{off}}$. This

points to the dual role of certain parameters. For example, while increasing the particle radius increases mq_{on}/Γ (since $m \propto R^3$ and $\Gamma \sim R$), it decreases $k/\Gamma q_{off}$, and hence an optimal particle radius is needed. Furthermore, while shorter polymer lengths increase stiffness k, they also increase hydrodynamic friction Γ through lubrication effects [36,37] and hence an optimal polymer length is also required. We elaborate in detail on the role of various experimental parameters in Sec. 4 of the Supplemental Material [3], and we provide a predictive tool for the rapid exploration of different material designs [83].

We estimate the change in diffusion coefficient as a function of temperature that using different cores would induce (Supplemental Material, Sec. 4), computing D_{eff} using Eq. (4). We compute the temperature dependence of N and q_{off} using a mean-field model that has been validated experimentally [31,48,84–86], observing that q_{on}, γ, Γ do not change significantly with temperature [52]. The difference between the diffusion coefficients of gold and polystyrene colloids is maximal at intermediate temperatures where colloids form only a few bonds ($\bar{N} = 1$–10) with the surface (Figs. S3–S6 in Supplemental Material [3]). Drawing parameters from existing particle systems, we predict the difference in diffusion coefficients to be 1%–2% (Fig. S3 in Supplemental Material [3]). While this is a small effect at the single-particle level, mass discrepancies between numerous particles, and hence diffusion coefficient discrepancies, could accumulate to impact collective properties such as nucleation, annealing (as was seen in a different context [87]) or trigger mass-dependent phase separations. Fine-tuning particle coatings, e.g., reducing the ligand length with commercially available ligands, could increase the difference in single-particle diffusion coefficients to 6%–7% (Figs. S4 and S5 in Supplemental Material [3]), which is well within experimental accuracy [20]. Exploiting further advanced experimental conditions such as changing the solvent [88,89] increases the discrepancy to 10%–20% (Fig. S6 in Supplemental Material [3]).

In summary, our model predicts that inertia could modify the diffusion coefficient of particles in fluids with ligand-receptor contacts, inducing a diffusion slowdown with increased inertia. The onset of the slowdown occurs when the binding timescale $\tau_{on} = q_{on}^{-1}$ is faster than the timescale for the inertial relaxation, which is $\tau_m = m/\Gamma$ in our model, a lower bound on the actual timescale since momentum decays algebraically in most fluid systems [2,5]. The magnitude of the inertial slowdown is increased with stiff ligands and fewer bound legs. Improvements to our model could include, among other things, fluid memory kernels to investigate the algebraic decay of momentum [2] or ligand density inhomogeneities to probe subdiffusive dynamics that are observed at low temperatures [47]. As the main principles inducing mass-dependent dynamics are essential to the account of ligand receptors, namely binding and unbinding and altered motion when bound, it is reasonable to assume that mass-dependent diffusion should persist in any ligand-receptor model. We predict the diffusion slowdown could be probed experimentally by fine-tuning DNA-coated colloids.

Our analysis thus provides a key principle to investigate the onset of inertial effects in other micronscale particles in liquids. When there exists a physical timescale in the system that is fast, and comparable to the relaxation of inertia, inertial effects *could* arise. This criterion is repeatedly observed in other contexts [2,4–6,21–27]. However, in general inertial effects do not necessarily imply that the diffusion coefficient depends on mass. For example, when a particle has an inertial relaxation time comparable to the relaxation time of the solvent, then the particle's velocity autocorrelation function decays algebraically instead of exponentially, but its diffusion coefficient remains independent of inertia [2]. Hence, an overdamped equilibrium system where single-particle diffusion depends on mass remains surprising.

Targeted experiments, especially on particles with ligand-receptor contacts, could identify other inertial effects beyond diffusion slowdown. For DNA-coated colloids, one could envision that such inertia-modified dynamics could also impact collective properties such as crystallographic alignment into self-assembled structures [40,90]. Understanding the dynamics of such complex micronscale particles is a key step to pave the way toward controlled design at the microscale, e.g., to improve synthesis of materials with advanced optical properties [91,92].

The authors thank Brennan Sprinkle for sharing his code to calculate lubrication forces, and Aleksandar Donev for fruitful discussions. S. M. received funding from the European Union's Horizon 2020 research and innovation programme under the Marie Skłodowska-Curie Grant Agreement No. 839225, Molecular Control. All authors were supported in part by the MRSEC Program of the National Science Foundation under Grant No. DMR-1420073. M. H.-C. was partially supported by the US Department of Energy under Award No. DE-SC0012296, by Grant No. NSF-DMS-2111163, and acknowledges support from the Alfred P. Sloan Foundation.

*Corresponding author.
sophie@marbach.fr
†Corresponding author.
holmes@cims.nyu.edu

[1] M. E. Cates and V. N. Manoharan, Celebrating Soft Matter 's 10th anniversary: Testing the foundations of classical entropy: Colloid experiments, Soft Matter **11**, 6538 (2015).
[2] X. Bian, C. Kim, and G. E. Karniadakis, 111 years of Brownian motion, Soft Matter **12**, 6331 (2016).

[3] See Supplemental Material at http://link.aps.org/supplemental/10.1103/PhysRevLett.129.048003 for additional information on simulation methods, for analytical details on the coarse-graining procedure and analytical assumptions, for references and numbers used to establish Fig. 3 and finally for the calculation procedure used to evaluate the diffusion coefficients of light and heavy DNA-coated colloids.
[4] J. Schmidt and J. Skinner, Hydrodynamic boundary conditions, the stokes–Einstein law, and long-time tails in the Brownian limit, J. Chem. Phys. **119**, 8062 (2003).
[5] F. Balboa Usabiaga, X. Xie, R. Delgado-Buscalioni, and A. Donev, The stokes-Einstein relation at moderate schmidt number, J. Chem. Phys. **139**, 214113 (2013).
[6] H. Löwen, Inertial effects of self-propelled particles: From active Brownian to active langevin motion, J. Chem. Phys. **152**, 040901 (2020).
[7] R. J. Macfarlane, B. Lee, M. R. Jones, N. Harris, G. C. Schatz, and C. A. Mirkin, Nanoparticle superlattice engineering with dna, Science **334**, 204 (2011).
[8] W. B. Rogers, W. M. Shih, and V. N. Manoharan, Using DNA to program the self-assembly of colloidal nanoparticles and microparticles, Nat. Rev. Mater. **1**, 16008 (2016).
[9] D. J. Lewis, L. Z. Zornberg, D. J. Carter, and R. J. Macfarlane, Single-crystal winterbottom constructions of nanoparticle superlattices, Nat. Mater. **19**, 719 (2020).
[10] M. Mammen, S.-K. Choi, and G. M. Whitesides, Polyvalent interactions in biological systems: Implications for design and use of multivalent ligands and inhibitors, Angew. Chem., Int. Ed. Engl. **37**, 2754 (1998).
[11] T. Sakai, S. I. Nishimura, T. Naito, and M. Saito, Influenza a virus hemagglutinin and neuraminidase act as novel motile machinery, Sci. Rep. **7**, 1 (2017).
[12] T. Sakai, H. Takagi, Y. Muraki, and M. Saito, Unique directional motility of influenza c virus controlled by its filamentous morphology and short-range motions, J. Virol. **92**, e01522 (2018).
[13] M. Müller, D. Lauster, H. H. Wildenauer, A. Herrmann, and S. Block, Mobility-based quantification of multivalent virus-receptor interactions: New insights into influenza a virus binding mode, Nano Lett. **19**, 1875 (2019).
[14] R. Alon and S. Feigelson, From rolling to arrest on blood vessels: Leukocyte tap dancing on endothelial integrin ligands and chemokines at sub-second contacts, in *Seminars in Immunology* (Elsevier, New York, 2002), Vol. 14, pp. 93–104.
[15] K. Ley, C. Laudanna, M. I. Cybulsky, and S. Nourshargh, Getting to the site of inflammation: The leukocyte adhesion cascade updated, Nat. Rev. Immunol. **7**, 678 (2007).
[16] C. B. Korn and U. S. Schwarz, Dynamic states of cells adhering in shear flow: From slipping to rolling, Phys. Rev. E **77**, 041904 (2008).
[17] P. C. Bressloff and J. M. Newby, Stochastic models of intracellular transport, Rev. Mod. Phys. **85**, 135 (2013).
[18] D. A. Hammer, Adhesive dynamics, J. Biomech. Eng. **136**, 021006 (2014).
[19] U. S. Schwarz and R. Alon, L-selectin-mediated leukocyte tethering in shear flow is controlled by multiple contacts and cytoskeletal anchorage facilitating fast rebinding events, Proc. Natl. Acad. Sci. U.S.A. **101**, 6940 (2004).
[20] S. Marbach, J. A. Zheng, and M. Holmes-Cerfon, The nanocaterpillar's random walk: Diffusion with ligand-receptor contacts, Soft Matter **18**, 3130 (2022).
[21] T. Li and M. G. Raizen, Brownian motion at short time scales, Ann. Phys. (Berlin) **525**, 281 (2013).
[22] A. Daddi-Moussa-Ider, A. Guckenberger, and S. Gekle, Long-lived anomalous thermal diffusion induced by elastic cell membranes on nearby particles, Phys. Rev. E **93**, 012612 (2016).
[23] M. Trulsson, B. Andreotti, and P. Claudin, Transition from the Viscous to Inertial Regime in Dense Suspensions, Phys. Rev. Lett. **109**, 118305 (2012).
[24] F. Boyer, É. Guazzelli, and O. Pouliquen, Unifying Suspension and Granular Rheology, Phys. Rev. Lett. **107**, 188301 (2011).
[25] V. Démery, Mean-field microrheology of a very soft colloidal suspension: Inertia induces shear thickening, Phys. Rev. E **91**, 062301 (2015).
[26] C. Dai, I. R. Bruss, and S. C. Glotzer, Phase separation and state oscillation of active inertial particles, Soft Matter **16**, 2847 (2020).
[27] B. Lindner, L. Schimansky-Geier, P. Reimann, P. Hänggi, and M. Nagaoka, Inertia ratchets: A numerical study versus theory, Phys. Rev. E **59**, 1417 (1999).
[28] N. Dorsaz, C. De Michele, F. Piazza, and G. Foffi, Inertial effects in diffusion-limited reactions, J. Phys. Condens. Matter **22**, 104116 (2010).
[29] F. Piazza, G. Foffi, and C. De Michele, Irreversible bimolecular reactions with inertia: From the trapping to the target setting at finite densities, J. Phys. Condens. Matter **25**, 245101 (2013).
[30] J. P. Lee-Thorp and M. Holmes-Cerfon, Modeling the relative dynamics of dna-coated colloids, Soft Matter **14**, 8147 (2018).
[31] M. Rubinstein, R. H. Colby *et al.*, *Polymer Physics* (Oxford University Press, New York, 2003), Vol. 23.
[32] E. Miller, T. Garcia, S. Hultgren, and A. F. Oberhauser, The mechanical properties of e. coli type 1 pili measured by atomic force microscopy techniques, Biophys. J. **91**, 3848 (2006).
[33] R. Y. Lim, N.-P. Huang, J. Köser, J. Deng, K. A. Lau, K. Schwarz-Herion, B. Fahrenkrog, and U. Aebi, Flexible phenylalanine-glycine nucleoporins as entropic barriers to nucleocytoplasmic transport, Proc. Natl. Acad. Sci. U.S.A. **103**, 9512 (2006).
[34] G. Pavliotis and A. Stuart, *Multiscale Methods: Averaging and Homogenization* (Springer Science & Business Media, New York, 2008).
[35] B. Fogelson and J. P. Keener, Enhanced nucleocytoplasmic transport due to competition for elastic binding sites, Biophys. J. **115**, 108 (2018).
[36] A. J. Goldman, R. G. Cox, and H. Brenner, Slow viscous motion of a sphere parallel to a plane wall—i motion through a quiescent fluid, Chem. Eng. Sci. **22**, 637 (1967).
[37] B. Sprinkle, E. B. Van Der Wee, Y. Luo, M. M. Driscoll, and A. Donev, Driven dynamics in dense suspensions of microrollers, Soft Matter **16**, 7982 (2020).
[38] R. W. Perry, M. C. Holmes-Cerfon, M. P. Brenner, and V. N. Manoharan, Two-Dimensional Clusters of Colloidal

Spheres: Ground States, Excited States, and Structural Rearrangements, Phys. Rev. Lett. **114**, 228301 (2015).
[39] F. B. Usabiaga, R. Delgado-Buscalioni, B. E. Griffith, and A. Donev, Inertial coupling method for particles in an incompressible fluctuating fluid, Comput. Methods Appl. Mech. Eng. **269**, 139 (2014).
[40] M. Holmes-Cerfon, Stochastic disks that roll, Phys. Rev. E **94**, 052112 (2016).
[41] Y. Bae, S. Lee, J. Kim, and H. Jeong, Inertial effects on the Brownian gyrator, Phys. Rev. E **103**, 032148 (2021).
[42] E. Vanden-Eijnden and G. Ciccotti, Second-order integrators for langevin equations with holonomic constraints, Chem. Phys. Lett. **429**, 310 (2006).
[43] B. Fogelson and J. P. Keener, Transport facilitated by rapid binding to elastic tethers, SIAM J. Appl. Math. **79**, 1405 (2019).
[44] G. A. Pavliotis, *Stochastic Processes and Applications: Diffusion Processes, the Fokker-Planck and Langevin Equations* (Springer, New York, 2014), Vol. 60.
[45] A. Schallamach, A theory of dynamic rubber friction, Wear **6**, 375 (1963).
[46] K. Tawada and K. Sekimoto, Protein friction exerted by motor enzymes through a weak-binding interaction, J. Theor. Biol. **150**, 193 (1991).
[47] Q. Xu, L. Feng, R. Sha, N. C. Seeman, and P. M. Chaikin, Subdiffusion of a Sticky Particle on a Surface, Phys. Rev. Lett. **106**, 228102 (2011).
[48] F. Cui, S. Marbach, J. Zheng, M. Holmes-Cerfon, and D. S. Pine, Comprehensive view of microscopic interactions between DNA-coated colloids, Nat. Coomun **13**, 2304 (2022).
[49] N. K. Sauter, M. D. Bednarski, B. A. Wurzburg, J. E. Hanson, G. M. Whitesides, J. J. Skehel, and D. C. Wiley, Hemagglutinins from two influenza virus variants bind to sialic acid derivatives with millimolar dissociation constants: A 500-mhz proton nuclear magnetic resonance study, Biochemistry **28**, 8388 (1989).
[50] V. Reiter-Scherer, J. L. Cuellar-Camacho, S. Bhatia, R. Haag, A. Herrmann, D. Lauster, and J. P. Rabe, Force spectroscopy shows dynamic binding of influenza hemagglutinin and neuraminidase to sialic acid, Biophys. J. **116**, 1037 (2019).
[51] Y. Wang, Y. Wang, X. Zheng, É. Ducrot, J. S. Yodh, M. Weck, and D. J. Pine, Crystallization of dna-coated colloids, Nat. Commun. **6**, 1 (2015).
[52] J. X. Zhang, J. Z. Fang, W. Duan, L. R. Wu, A. W. Zhang, N. Dalchau, B. Yordanov, R. Petersen, A. Phillips, and D. Y. Zhang, Predicting dna hybridization kinetics from sequence, Nat. Chem. **10**, 91 (2018).
[53] S. Y. Park, A. K. Lytton-Jean, B. Lee, S. Weigand, G. C. Schatz, and C. A. Mirkin, Dna-programmable nanoparticle crystallization, Nature (London) **451**, 553 (2008).
[54] H. H. Fakih, M. M. Itani, and P. Karam, Gold nanoparticles-coated polystyrene beads for the multiplex detection of viral dna, Sens. Actuators B **250**, 446 (2017).
[55] S. J. Hurst, A. K. Lytton-Jean, and C. A. Mirkin, Maximizing dna loading on a range of gold nanoparticle sizes, Anal. Chem. **78**, 8313 (2006).
[56] H. Ting-Beall, D. Needham, and R. Hochmuth, Volume and osmotic properties of human neutrophils., Blood **81**, 2774 (1993).
[57] J.-Y. Shao, H. P. Ting-Beall, and R. M. Hochmuth, Static and dynamic lengths of neutrophil microvilli, Proc. Natl. Acad. Sci. U.S.A. **95**, 6797 (1998).
[58] O. Dwir, A. Solomon, S. Mangan, G. S. Kansas, U. S. Schwarz, and R. Alon, Avidity enhancement of l-selectin bonds by flow: Shear-promoted rotation of leukocytes turn labile bonds into functional tethers, J. Cell Biol. **163**, 649 (2003).
[59] J. Fritz, A. G. Katopodis, F. Kolbinger, and D. Anselmetti, Force-mediated kinetics of single p-selectin/ligand complexes observed by atomic force microscopy, Proc. Natl. Acad. Sci. U.S.A. **95**, 12283 (1998).
[60] P. Mehta, R. D. Cummings, and R. P. McEver, Affinity and kinetic analysis of p-selectin binding to p-selectin glycoprotein ligand-1, J. Biol. Chem. **273**, 32506 (1998).
[61] R. Alon, D. A. Hammer, and T. A. Springer, Lifetime of the p-selectin-carbohydrate bond and its response to tensile force in hydrodynamic flow, Nature (London) **374**, 539 (1995).
[62] R. Alon, S. Chen, K. D. Puri, E. B. Finger, and T. A. Springer, The kinetics of l-selectin tethers and the mechanics of selectin-mediated rolling, J. Cell Biol. **138**, 1169 (1997).
[63] S. Bakshi, A. Siryaporn, M. Goulian, and J. C. Weisshaar, Superresolution imaging of ribosomes and rna polymerase in live escherichia coli cells, Mol. Microbiol. **85**, 21 (2012).
[64] S. Chen and T. A. Springer, Selectin receptor–ligand bonds: Formation limited by shear rate and dissociation governed by the bell model, Proc. Natl. Acad. Sci. U.S.A. **98**, 950 (2001).
[65] O. Yakovenko, V. Tchesnokova, E. V. Sokurenko, and W. E. Thomas, Inactive conformation enhances binding function in physiological conditions, Proc. Natl. Acad. Sci. U.S.A. **112**, 9884 (2015).
[66] M. M. Sauer, R. P. Jakob, T. Luber, F. Canonica, G. Navarra, B. Ernst, C. Unverzagt, T. Maier, and R. Glockshuber, Binding of the bacterial adhesin fimh to its natural, multivalent high-mannose type glycan targets, J. Am. Chem. Soc. **141**, 936 (2019).
[67] M. M. Sauer, R. P. Jakob, J. Eras, S. Baday, D. Eriş, G. Navarra, S. Berneche, B. Ernst, T. Maier, and R. Glockshuber, Catch-bond mechanism of the bacterial adhesin fimh, Nat. Commun. **7**, 10738 (2016).
[68] F. C. Neidhardt, J. L. Ingraham, and M. Schaechter, *Physiology of the Bacterial Cell; A Molecular Approach*, 589.901 N397 (Sinauer Associates, Ann Arbor, 1990).
[69] C. B. Korn, S. Klumpp, R. Lipowsky, and U. S. Schwarz, Stochastic simulations of cargo transport by processive molecular motors, J. Chem. Phys. **131**, 245107 (2009).
[70] F. Gibbons, J.-F. Chauwin, M. Despósito, and J. V. José, A dynamical model of kinesin-microtubule motility assays, Biophys. J. **80**, 2515 (2001).
[71] J. Wu, A. H. Corbett, and K. M. Berland, The intracellular mobility of nuclear import receptors and nls cargoes, Biophys. J. **96**, 3840 (2009).
[72] I. V. Aramburu and E. A. Lemke, Floppy but not sloppy: Interaction mechanism of fg-nucleoporins and nuclear

transport receptors, in *Seminars in Cell & Developmental Biology* (Elsevier, New York, 2017), Vol. 68, pp. 34–41.
[73] A. Radu, G. Blobel, and M. S. Moore, Identification of a protein complex that is required for nuclear protein import and mediates docking of import substrate to distinct nucleoporins, Proc. Natl. Acad. Sci. U.S.A. **92**, 1769 (1995).
[74] S. Milles, D. Mercadante, I. V. Aramburu, M. R. Jensen, N. Banterle, C. Koehler, S. Tyagi, J. Clarke, S. L. Shammas, M. Blackledge *et al.*, Plasticity of an ultrafast interaction between nucleoporins and nuclear transport receptors, Cell **163**, 734 (2015).
[75] L.-C. Tu, G. Fu, A. Zilman, and S. M. Musser, Large cargo transport by nuclear pores: Implications for the spatial organization of fg-nucleoporins, EMBO J. **32**, 3220 (2013).
[76] A. Harris, G. Cardone, D. C. Winkler, J. B. Heymann, M. Brecher, J. M. White, and A. C. Steven, Influenza virus pleiomorphy characterized by cryoelectron tomography, Proc. Natl. Acad. Sci. U.S.A. **103**, 19123 (2006).
[77] C. Sieben, C. Kappel, R. Zhu, A. Wozniak, C. Rankl, P. Hinterdorfer, H. Grubmüller, and A. Herrmann, Influenza virus binds its host cell using multiple dynamic interactions, Proc. Natl. Acad. Sci. U.S.A. **109**, 13626 (2012).
[78] M. Laue, A. Kauter, T. Hoffmann, L. Möller, J. Michel, and A. Nitsche, Morphometry of sars-cov and sars-cov-2 particles in ultrathin plastic sections of infected vero cell cultures, Sci. Rep. **11**, 3515 (2021).
[79] J. Yang, S. J. Petitjean, M. Koehler, Q. Zhang, A. C. Dumitru, W. Chen, S. Derclaye, S. P. Vincent, P. Soumillion, and D. Alsteens, Molecular interaction and inhibition of sars-cov-2 binding to the ace2 receptor, Nat. Commun. **11**, 1 (2020).
[80] A. C. Walls, Y.-J. Park, M. A. Tortorici, A. Wall, A. T. McGuire, and D. Veesler, Structure, function, and antigenicity of the sars-cov-2 spike glycoprotein, Cell **181**, 281 (2020).
[81] R. D. Vale, T. Funatsu, D. W. Pierce, L. Romberg, Y. Harada, and T. Yanagida, Direct observation of single kinesin molecules moving along microtubules, Nature (London) **380**, 451 (1996).
[82] S. Sacanna and A. P. Philipse, A generic single-step synthesis of monodisperse core/shell colloids based on spontaneous pickering emulsification, Adv. Mater. **19**, 3824 (2007).
[83] Our tool is available through GitHub,10.5281/zenodo.6798435.
[84] S. T. Milner, T. A. Witten, and M. E. Cates, Theory of the grafted polymer brush, Macromolecules **21**, 2610 (1988).
[85] J. SantaLucia, A unified view of polymer, dumbbell, and oligonucleotide DNA nearest-neighbor thermodynamics, Proc. Natl. Acad. Sci. U.S.A. **95**, 1460 (1998).
[86] H. Chen, S. P. Meisburger, S. A. Pabit, J. L. Sutton, W. W. Webb, and L. Pollack, Ionic strength-dependent persistence lengths of single-stranded RNA and DNA, Proc. Natl. Acad. Sci. U.S.A. **109**, 799 (2012).
[87] S. Ramananarivo, E. Ducrot, and J. Palacci, Activity-controlled annealing of colloidal monolayers, Nat. Commun. **10**, 3380 (2019).
[88] J. W. Thompson, T. J. Kaiser, and J. W. Jorgenson, Viscosity measurements of methanol–water and acetonitrile–water mixtures at pressures up to 3500 bar using a novel capillary time-of-flight viscometer, J. Chromatogr. A **1134**, 201 (2006).
[89] S.-i. Nakano and N. Sugimoto, The structural stability and catalytic activity of dna and rna oligonucleotides in the presence of organic solvents, Biophys. Rev. Lett. **8**, 11 (2016).
[90] I. C. Jenkins, M. T. Casey, J. T. McGinley, J. C. Crocker, and T. Sinno, Hydrodynamics selects the pathway for displacive transformations in dna-linked colloidal crystallites, Proc. Natl. Acad. Sci. U.S.A. **111**, 4803 (2014).
[91] N. Vogel, S. Utech, G. T. England, T. Shirman, K. R. Phillips, N. Koay, I. B. Burgess, M. Kolle, D. A. Weitz, and J. Aizenberg, Color from hierarchy: Diverse optical properties of micron-sized spherical colloidal assemblies, Proc. Natl. Acad. Sci. U.S.A. **112**, 10845 (2015).
[92] M. He, J. P. Gales, É. Ducrot, Z. Gong, G.-R. Yi, S. Sacanna, and D. J. Pine, Colloidal diamond, Nature (London) **585**, 524 (2020).